e-ISSN: 2149-4584

Erzincan University Journal of Science and Technology

EJSAT 2026, 19 (1) 26-50

Research Article

Comprehensive Energy and Exergy Analysis of an Integrated Organic Rankine Cycle (ORC) and Vapour Compression Cycle (VCC) with Proton Exchange Membrane (PEM) Electrolyzer

Cenker Aktemur[1*]

[1]Sivas University of Science and Technology, Faculty of Engineering and Natural Sciences, Mechanical Engineering Department, 58000, Sivas, Türkiye

Received: 11/12/2025, **Revised:** 09/03/2026, **Accepted:** 23/03/2026, **Published:** 30/03/2026

Abstract

The present study focuses on the thermodynamic performance of a novel integrated Organic Rankine cycle-Vapor Compression cycle- Proton Exchange Membrane (ORC–VCC–PEM) system for simultaneous power production, cooling, and hydrogen generation. The rationale behind this study is to address the need for efficient utilization of low-grade heat sources and the scarcity of research work related to the integration of ORC, VCC, and PEM technologies using a unified framework of energy and exergy analysis. To achieve this, a fully integrated system is proposed with the internal heat exchanger designed as a cascade heat exchanger to couple the ORC and VCC. Furthermore, a detailed screening of 188 different working fluid pairs is carried out to determine the most thermodynamically compatible pair of fluids, for which Dimethylether-Toluene is found to be the most suitable. Parametric analyses are conducted to determine the impact of critical operating parameters. The study reveals that increasing the evaporator temperature significantly improves the performance of the system, resulting in a 17.1% enhancement in the overall net Coefficient of Performance (COP) of the system and a corresponding 11.2% decrease in total exergy destruction. Conversely, increasing the condensing temperature reduces the performance of the system substantially, resulting in a notable decrease in overall net COP and a large decrease of 32% in hydrogen production. Additionally, increasing the temperature difference in the internal heat exchanger leads to increased thermal irreversibility, resulting in increased exergy destruction and decreased system efficiency. Further analysis of the system reveals that the expansion valve and the compressor contribute most to exergy destruction in the system. The main contribution of the present work is the development of a proposed ORC–VCC–PEM system using a unified framework of thermodynamic performance analysis and a detailed assessment of working fluids.

Keywords: Organic Rankine Cycle, Vapor Compression Cycle, Proton Exchange Membrane

Öz

Bu çalışma, eş zamanlı güç üretimi, soğutma ve hidrojen üretimi sağlayan yeni bir entegre Organik Rankine Çevrimi–Buhar Sıkıştırmalı Çevrim–Proton Değişim Membranı (ORÇ–BSÇ–PDM) sisteminin termodinamik performansına odaklanmaktadır. Çalışmanın temel motivasyonu, düşük sıcaklıklı ısı kaynaklarının etkin kullanımına yönelik artan ihtiyaç ile ORÇ, BSÇ ve PDM teknolojilerinin enerji ve ekserji analizi açısından bütünleşik bir çerçevede ele alındığı çalışmaların sınırlı olmasıdır. Bu doğrultuda, ORÇ ve BSÇ alt sistemlerini birbirine bağlayan iç ısı değiştiricinin kaskad bir ısı değiştirici olarak tasarlandığı tam entegre bir sistem önerilmiştir. Ayrıca, termodinamik açıdan en uyumlu akışkan çiftini belirlemek amacıyla 188 farklı çalışma akışkanı çifti detaylı şekilde incelenmiş ve en uygun kombinasyonun Dimetil eter–Toluen olduğu belirlenmiştir. Kritik işletme parametrelerinin etkisini ortaya koymak amacıyla parametrik analizler gerçekleştirilmiştir. Elde edilen sonuçlar, evaporatör sıcaklığının artmasının sistem performansını önemli ölçüde iyileştirdiğini, toplam net soğutma performans katsayısında (STK) %17,1 artış ve toplam ekserji yıkımında %11,2 azalma sağladığını göstermektedir. Buna karşılık, yoğuşturucu sıcaklığındaki artış sistem performansını belirgin şekilde düşürmekte, net STK'Da azalmaya ve hidrojen üretiminde yaklaşık %32 oranında ciddi bir düşüşe yol açmaktadır. Ayrıca, iç ısı değiştiricisindeki sıcaklık farkının artması, termal tersinmezlikleri artırarak daha yüksek ekserji yıkımına ve sistem veriminde azalmaya neden olmaktadır. Sistem bileşenleri bazında yapılan analizler, ekserji yıkımına en fazla katkının genleşme vanası ve kompresörden kaynaklandığını ortaya koymaktadır. Bu çalışmanın temel katkısı, ORÇ–BSÇ–PDM sisteminin birleşik bir termodinamik ve ekserji analiz çerçevesi altında geliştirilmesi ve çalışma akışkanlarının kapsamlı bir şekilde değerlendirilmesidir.

Anahtar Kelimeler: Organik Rankine Çevrimi, Buhar Sıkıştırmalı Çevrim, Proton Değişim Membranı

***Corresponding Author**: cenker.aktemur@sivas.edu.tr

Cite this Article: Erzincan University Journal of Science and Technology 2026, 19(1)26-50. https://doi.org/10.18185/erzifbed.1840352

1.Introduction

The Organic Rankine Cycle (ORC) facilitates the effective utilization of low-temperature heat sources such as biomass energy [1], industrial waste heat [2], solar energy [3], and geothermal energy [4] for electric generation. However, the low efficiency, which is a drawback of the ORC, restricts its application to only low-temperature heat sources for electric power generation. On the other hand, the need for increased amounts of electric energy for refrigeration has led to the utilization of air conditioning systems. This results in 15% of total electric energy consumption globally for air conditioning [6, 7]. Keeping these issues in mind, the concept of the ORC-VCC system has been introduced. This system utilizes low-temperature heat sources in the refrigeration sector, which has potential application either in the refrigeration process or electric generation [8].

Screening of working fluids is one of the primary areas of concern in present day ORC-VCC systems. The thermo-economic evaluation of the system was performed by Zhar et al. [9] using R123, R11, and R113, but the authors finally recommended the use of R123. Among the various working fluids shortlisted, Javanshir et al. [10] noted that R22 demonstrated better cooling rates and reduced irreversibility, while R134a resulted in lower total cost of operation. Besides, Nasir et al. [11] believed that R134a was the best working fluid for the said system. However, the recommended working fluids in the literature demonstrate higher global warming potential and are projected to be progressively removed from the marketplace in the years to come. Consequently, a search for low GWP refrigerants has been started by a number of investigators for the said application. Describing their thermodynamic properties, the suitable working fluid for the said application has been reported to be R600 by Li et al. [12]. For an ORC-VCC system assisted by solar and ocean energy, Rami and Allouhi [13] drew similar inferences regarding R600 working fluid, declaring the highest exergy and energy efficiencies, respectively. Using multi-layer optimization methods, Xia et al. [14] demonstrated R602 to be the best fluid in the said application for the various heat sources. For the said application, the thermo-economic optimization of various working fluids has been performed through grey relational analysis by Wang et al. [15] and the best fluid found to be R601.

Various studies have carried out the parametric investigation of the ORC-VCC system. Karellas and Brainakis [16] suggest that an increase in the VCC evaporation temperature leads to an increase in exergy efficiency and COP, while an increase in the condensation temperature has a reverse effect. Qureshi et al. [17] declare that the evaporation temperature of the ORC system is an important factor in determining the performance of the solar assisted ORC-VCC system. Xia et al. [18] investigated the effects of the R601a/R602 mixture ratio in the system, and based upon their findings, the maximum thermodynamic performance of the system is possible at a mixture ratio of 0.4/0.6. Asim et al. [19] proved that an increase in the temperature on the chilled water side increases the COP, but an increase in the cooling water temperature has a negative impact. Nasir et al. [20] proved the influence of flow rates and subcooling on the organic rankine cycle in absorbing refrigerant heat. The results have clearly shown that flow rates and subcooling have a significant influence. Saleh [21] proved that an increase in temperature as

well as the intensity of the heat source increases the COP. Apart from these studies, various researchers have carried out optimization studies on ORC-VCC systems. Wang et al. [22] carried out a multi-objective optimization study on ORC-VCC systems. The results showed that optimum operating conditions are obtained with a 32% improvement in cooling capacity as well as a 14% improvement in COP. Sun et al. [23] carried out optimization studies on organic rankine cycle-vapor compression refrigeration systems under various conditions. The results have been obtained using the annualized total cost as an objective function. Notwithstanding, the existing studies as well as results have mostly concentrated on optimization under various conditions. Barac et al. [24] carried out a thermo-economic optimization study on organic rankine cycle-vapor compression refrigeration systems. It has to be noted that most of these studies are carried out under assumptions that are mostly hypothetical. Therefore, there are substantial differences between actual conditions as well as results.

To the authors' best knowledge, there is no previous report in literature of a tri-generation system that combines ORC, VCC, and PEM electrolysis. This study proposes an integrated system of ORC-VCC-PEM for tri-generation of electrical power, refrigeration, and hydrogen production. The main contributions of this study are briefly described in the following:

- A proposed tri-generation configuration that combines an ORC, a VCC, and a PEM electrolyzer is proposed to simultaneously produce electricity, cooling, and hydrogen using low-grade thermal energy sources.
- An extensive screening of 188 working fluid combinations is conducted to determine the most promising thermodynamic working fluid pair for the proposed integrated cycle configuration.
- Based on the results of the most promising thermodynamic working fluid pair, a thorough thermodynamic assessment of the proposed integrated ORC-VCC-PEM system is conducted using energy and exergy analyses.
- The proposed work aims to elucidate the thermodynamic interactions of the power generation, cooling generation, and hydrogen generation processes and identify the major irreversibilities in the proposed integrated system configuration.
- The proposed work provides useful insights into the design and optimization of advanced tri-generation systems that exploit low-grade thermal energy sources.

2. Methodology

2.1 Modelling, system boundaries and component interactions

Figure 1 shows the conceptual configuration of the integrated ORC-VCC system with the PEM electrolyzer, highlighting the flow of the working fluid and the interactions between the main system components. As illustrated in Figure 1, the ORC subsystem uses the low-grade thermal energy to generate electricity through the turbine generator unit. The electricity generated by the ORC subsystem is transferred directly to the PEM electrolyzer. This enables the production of green hydrogen through the water electrolysis process. The VCC ssubystem uses the

electrical compressor to generate the refrigeration effect through the evaporator (1–4), whereas the heat rejection process occurs through the condenser (6–7). An internal heat exchanger (2–5–8–3) is also integrated to enhance the thermal interaction between the system components.

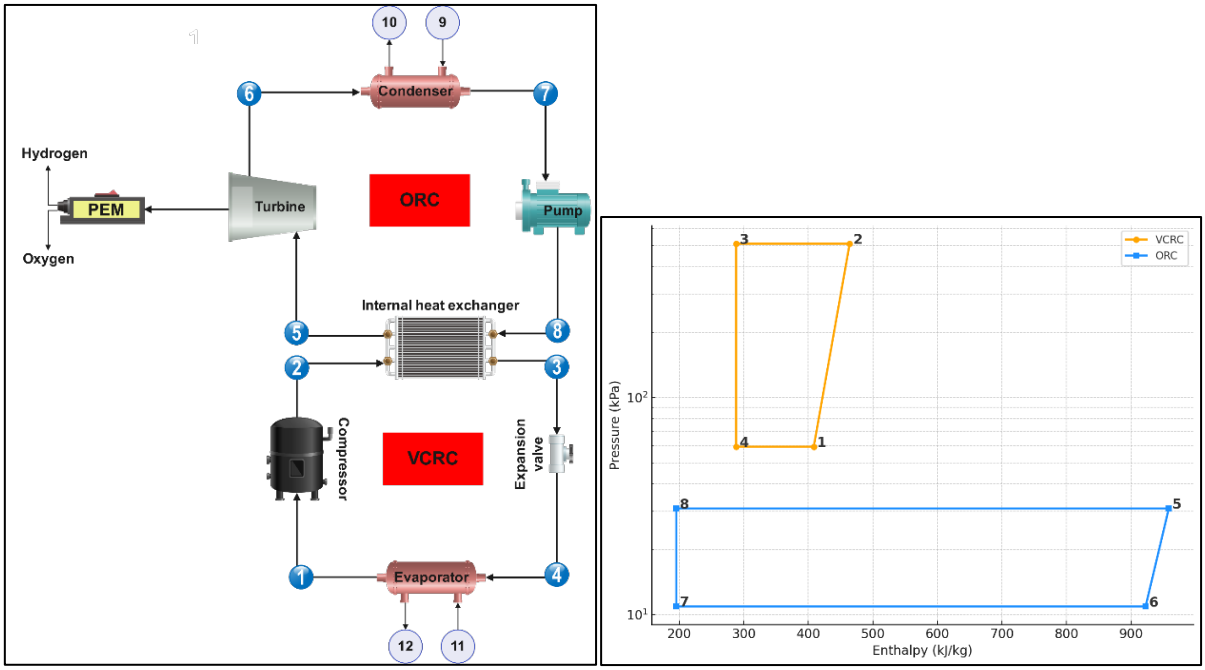

Figure 1. Schematic presentation of (a) an integrated VCC-ORC with PEM electrolyzer (b) lnP-h diagram of an integrated VCC-ORC system

The system boundaries include all major components in the integrated system with the ORC-VCC-PEM configuration. These components are the pump, evaporator, turbine, condenser, compressor, expansion valve, internal heat exchanger (IHE), and PEM electrolyzer. The ORC and VCC are thermally coupled via the IHE. The IHE acts as a cascade heat exchanger where energy is transferred from the hot side of the ORC to the cold side of the VCC. The PEM system is integrated with the ORC and utilizes the electric energy to produce hydrogen. Heat and mass interactions among system components are modeled under steady-state conditions with no changes in kinetic and potential energy.

2.2. Modeling approach and assumptions

The subsequent assumptions are utilized to simplify the thermodynamic modeling of the systems under consideration [25,26]:

- The systems are assumed to be under steady-state operation.
- The changes in kinetic energy, potential energy, and exergy are neglected.
- The pressure loss is neglected in the piping system.
- The pumps and turbines are treated as adiabatic machines with given isentropic efficiency.

Table 1 lists input parameters and values, Table 2 list mass and energy balance equations of ORC-VCC, Table 3 lists energy performance parameters of ORC-VCC, Table 4 lists exergy performance parameters of ORC-VCC-PEM system and Table 5 lists PEM electrolyzer model.

Table 1. Input parameters and values [25-27]

Parameter	Value
Evaporator temperature	5-10°C
Outlet temperature of VCC condenser	70°C
Condenser temperature	30-40°C
Temperature difference of VCC condenser and ORC evaporator	5-15 °C
Compressor isentropic efficiency	$0.874+0.0135(P_2/P_1)$
Turbine isentropic efficiency	0.85
Pump isentropic efficiency	0.80
Dead state temperature and pressure	25°C and 101.325 kPa
PEM electrolyzer operating temperature	80°C
PEM electrolyzer operating pressure	1 bar
Reference cathodic exchange current density	4600 A/m²
Reference anodic exchange current density	170000 A/m²
Activation energy of the anode reaction	76 kJ/mol
Activation energy of the cathode reaction	18 kJ/mol
Membrane thickness	100 μm
Water content of the membrane at the anode side	10
Water content of the membrane at the cathode side	14
Active surface area of the PEM electrolyzer cell	0.01 m²
Operating current density of the PEM electrolyzer	5000 A/m²
Faraday constant	96485 C/mol

Table 2. Mass and energy balance equations of ORC-VCC [25-27]

Component	Mass balance	Energy balance
Condenser	$\dot{m}_6=\dot{m}_7$ $\dot{m}_9=\dot{m}_{10}$	$\dot{Q}_{cond}=\dot{m}_6h_6-\dot{m}_7h_7$ $\dot{Q}_{cond,w}=\dot{m}_{10}h_{10}-\dot{m}_9h_9$
Pump	$\dot{m}_7=\dot{m}_8$	$\dot{W}_{turb}=\frac{\dot{m}_8h_{8s}-\dot{m}_7h_7}{\eta_{pump}}$
Turbine	$\dot{m}_5=\dot{m}_6$	$\dot{W}_{turb}=(\dot{m}_5h_5-\dot{m}_6h_{6s})\eta_{turb}$
Internal heat exchanger	$\dot{m}_2=\dot{m}_3$ $\dot{m}_5=\dot{m}_8$	$\dot{Q}_{IHE}=\dot{m}_5h_5-\dot{m}_8h_8$ $\dot{m}_2h_2-\dot{m}_3h_3=\dot{m}_5h_5-\dot{m}_8h_8$
Throttle valve	$\dot{m}_3=\dot{m}_4$	$h_3=h_4$
Compressor	$\dot{m}_1=\dot{m}_2$	$\dot{W}_{comp}=\frac{\dot{m}_2h_{2s}-\dot{m}_1h_1}{\eta_{comp}}$
Evaporator	$\dot{m}_1=\dot{m}_4$ $\dot{m}_{11}=\dot{m}_{12}$	$\dot{Q}_{evap}=\dot{m}_1h_1-\dot{m}_4h_4$ $\dot{Q}_{evap,w}=\dot{m}_{11}h_{11}-\dot{m}_{12}h_{12}$

Table 3. Energy performance parameters of ORC-VCC [25-27]

Parameter	Performance equation
Net ORC power	$\dot{W}_{net}=\dot{W}_{turb}-\dot{W}_{pump}$
Cooling COP of VCC	$COP_{VCC}=\frac{\dot{Q}_{evap}}{\eta_{comp}}$

Thermal efficiency of ORC	$\eta_{ORC}=\frac{\dot{W}_{net}}{\dot{Q}_{IHE}}$
Overall COP	$COP_{net}=\frac{\dot{Q}_{evap}}{\dot{W}_{comp}-\dot{W}_{net}}$

Table 4. Exergy performance parameters of ORC-VCC-PEM system [25-27]

Parameter	Exergy equation
Exergy efficiency of ORC	$\xi_{ORC}=\frac{\dot{W}_{net}}{\dot{E}_5 - \dot{E}_6}$
Exergy efficiency of VCC	$\xi_{VCC}=\frac{\dot{E}_{12} - \dot{E}_{11}}{\dot{W}_{comp}}$
Exergy efficiency of overall system	$\xi_{ORC}=\frac{\dot{E}_{12} - \dot{E}_{11} + \dot{E}_{H_2}}{\dot{W}_{comp}+\dot{W}_{pump}}$

Table 5. PEM electrolyzer model [26,27]

Parameter	PEM equation
Power consumption of PEM	$\dot{W}_{PEM}=V_{PEM}\times J\times A_{cell}\times n_{cell}$
PEM electrolyzer voltage	$V=V_0+V_{act,a}+V_{act,c}+V_{ohm}$
The reversible potential	$V_0=1.229-(8.5x10)^{-4}\times(T_{PEM}-298.15)$
Anode activation overpotential	$V_{act,a}=\frac{RT}{F}\sinh^{-1}\left(\frac{J}{2\times J_{0,a}}\right)$, $J_{0,a}=J_a^{ref}\exp\left(\frac{-E_{act,a}}{RT}\right)$
Cathode activation overpotential	$V_{act,c}=\frac{RT}{F}\sinh^{-1}\left(\frac{J}{2\times J_{0,c}}\right)$, $J_{0,c}=J_c^{ref}\exp\left(\frac{-E_{act,c}}{RT}\right)$
Ohmic overpotential	$V_{ohm}=R_{PEM}\times J$, $R_{PEM}=\int_0^D\frac{dx}{\sigma_{PEM}[\lambda(x)]}$
Mass flow rate of produced H_2	$\dot{n}_{H_2}=\frac{J_{PEM}A_{cell}n_{cell}}{2F}$, $\dot{m}_{H_2}=\dot{n}_{H_2}\times M_{H_2}$
Mass flow rate of produced O_2	$\dot{n}_{O_2}=\frac{J_{PEM}A_{cell}n_{cell}}{4F}\times10^{-3}$, $\dot{m}_{O_2}=\dot{n}_{O_2}\times M_{O_2}$

2.3. Calculation procedure and solution algorithm

The thermodynamic analysis is carried out in a step-by-step manner. In the first step, the thermodynamic states at all important points are calculated based on mass, energy and exergy balances. In the next step, the exergy destruction in individual components is calculated based on exergy balance equations. The system is analyzed in terms of turbin output, net COP, thermal efficiency, exergy destruction rate (system level and component-wise), exergy efficiency, and hydrogen production rate using design parameters such as condenser temperature, evaporator temperature and temperature difference in IHE. The overall calculation flow is structured as follows:

- Define input parameters
- Determine thermodynamic properties at all state points
- Solve ORC subsystem (pump → evaporator → turbine → IHE)

- Solve VCC subsystem (compressor → condenser → expansion valve → evaporator → IHE)
- Calculate PEM electrolyzer performance based on available electrical power
- Perform energy balance for each component
- Perform exergy analysis and compute exergy destruction for all components
- Evaluate system performance parameters (turbin output, thermal efficiency, COP_{net}, exergy efficiency,exergy destruction rate and hydrogen production rate)
- Conduct parametric analysis

This systematic and transparent modeling approach also ensures the reproducibility of results and a clear understanding of the interactions between the different components of the integrated system.

3. Results and Discussions

3.1. Selection of working fluid pair

This section provides the results of the thermodynamic performance of the proposed ORC-VCC + PEM system, based on the best suitable working fluid pair derived from the screening process of the 188 alternatives. The assessment of the 188 working fluid pairs is done to analyze and identify the best thermodynamic match, and then the best pair is analyzed in terms of energy and exergy assessments. Dimethylether-Toluene combination has been identified as the most beneficial working fluid combination when all the parameters are taken into consideration together, as it offers the best performance in terms of thermodynamic properties. To be more specific, Dimethylether-Toluene combination results in the maximum COP_{net}, the maximum overall $\eta_{ex,sys}$, while at the same time it results in the minimum $\dot{E}x_{total}$ among all possible combinations. This fact shows that the system is operating at its maximum energy utilization efficiency while at the same time minimizing the exergy destruction, indicating a perfectly balanced performance of all the ORC, VCC, and PEM systems combined together. This is mainly because of the good properties of Dimethylether working fluid in the VCC, as it improves the efficiency of the refrigeration cycle, while at the same time Toluene working fluid offers good stability in the ORC, allowing the efficient exploitation of low-grade heat sources.

Table 2. Performance analysis of the integrated VCC-ORC-PEM system for different sets of refrigerant combinations

VCC	ORC	$\dot{W}_{turb}$ (kW)	COP_{VCRC}	η_{ORC} (%)	COP_{net}	$m_{H_2,out}$ (g/h)	$\eta_{ex,sys}$	$\dot{E}x_{total}$ (kW)
R161	R1234yf	7.14	2.282	4.428	2.671	115.4	0.201	30.61
R161	R1243zf	7.169	2.282	4.564	2.685	118.9	0.2044	30.5
R161	R290	7.331	2.282	4.47	2.675	116.5	0.2012	30.58
R161	R600	6.996	2.282	4.708	2.7	122.7	0.209	30.38
R161	R600a	7.016	2.282	4.642	2.693	121	0.2071	30.43
R161	R1233zd(E)	6.964	2.282	4.752	2.704	123.8	0.2103	30.34
R161	HFO1336mzz(Z)	6.845	2.282	4.7	2.699	122.5	0.2095	30.39

R161	IsoPentane	6.908	2.282	4.734	2.702	123.4	0.2101	30.36
R161	N-PENTANE	6.865	2.282	4.721	2.701	123	0.2099	30.37
R161	Cyclohexane	7	2.282	4.857	2.715	126.6	0.2129	30.26
R161	Toluene	7.071	2.282	4.913	2.721	128	0.2141	30.21
R161	Isohexane	6.867	2.282	4.748	2.704	123.7	0.2107	30.35
R161	Isopropanol	7.069	2.282	4.91	2.721	127.9	0.214	30.21
R161	n-Hexane	6.797	2.282	4.707	2.7	122.7	0.2099	30.38
R161	n-Heptane	6.876	2.282	4.773	2.707	124.4	0.2113	30.33
R161	Dimethylether	7.149	2.282	4.69	2.698	122.2	0.2078	30.39
R152A	R161	7.225	2.348	4.596	2.775	118.8	0.2097	29.33
R152A	R1234yf	7.079	2.348	4.428	2.756	114.4	0.2059	29.46
R152A	R1243zf	7.109	2.348	4.564	2.771	117.9	0.2094	29.35
R152A	R290	7.269	2.348	4.47	2.761	115.5	0.2061	29.43
R152A	R600	6.937	2.348	4.708	2.787	121.6	0.2141	29.24
R152A	R600a	6.957	2.348	4.642	2.78	119.9	0.2122	29.29
R152A	R1233zd(E)	6.906	2.348	4.752	2.792	122.8	0.2155	29.2
R152A	HFO1336mzz(Z)	6.787	2.348	4.7	2.786	121.5	0.2147	29.24
R152A	IsoPentane	6.85	2.348	4.734	2.79	122.3	0.2153	29.21
R152A	N-PENTANE	6.807	2.348	4.721	2.788	122	0.2151	29.22
R152A	Cyclohexane	6.941	2.348	4.857	2.803	125.5	0.2182	29.11
R152A	Toluene	7.011	2.348	4.913	2.81	126.9	0.2194	29.07
R152A	Isohexane	6.809	2.348	4.748	2.791	122.7	0.2159	29.2
R152A	Isopropanol	7.009	2.348	4.91	2.809	126.9	0.2193	29.07
R152A	n-Hexane	6.74	2.348	4.707	2.787	121.6	0.2151	29.24
R152A	n-Heptane	6.818	2.348	4.773	2.794	123.3	0.2165	29.18
R152A	Dimethylether	7.089	2.348	4.69	2.785	121.2	0.2129	29.25
R1234ze(E)	R161	7.559	2.033	4.596	2.362	124.3	0.1855	35.55
R1234ze(E)	R152A	7.424	2.033	4.654	2.367	125.8	0.1873	35.5
R1234ze(E)	R1234yf	7.407	2.033	4.428	2.348	119.7	0.1821	35.69
R1234ze(E)	R1243zf	7.438	2.033	4.564	2.359	123.4	0.1852	35.58
R1234ze(E)	R290	7.606	2.033	4.47	2.351	120.8	0.1823	35.66
R1234ze(E)	R600	7.258	2.033	4.708	2.371	127.3	0.1893	35.46
R1234ze(E)	R600a	7.279	2.033	4.642	2.366	125.5	0.1876	35.51
R1234ze(E)	R1233zd(E)	7.225	2.033	4.752	2.375	128.5	0.1904	35.42
R1234ze(E)	HFO1336mzz(Z)	7.101	2.033	4.7	2.37	127.1	0.1897	35.46
R1234ze(E)	IsoPentane	7.167	2.033	4.734	2.373	128	0.1902	35.43
R1234ze(E)	N-PENTANE	7.122	2.033	4.721	2.372	127.6	0.1901	35.44
R1234ze(E)	Cyclohexane	7.263	2.033	4.857	2.384	131.3	0.1928	35.33
R1234ze(E)	Toluene	7.336	2.033	4.913	2.388	132.8	0.1939	35.28
R1234ze(E)	Isohexane	7.124	2.033	4.748	2.374	128.4	0.1908	35.42
R1234ze(E)	Isopropanol	7.334	2.033	4.91	2.388	132.7	0.1938	35.28
R1234ze(E)	n-Hexane	7.052	2.033	4.707	2.371	127.3	0.19	35.46
R1234ze(E)	n-Heptane	7.133	2.033	4.773	2.377	129	0.1913	35.4
R1234ze(E)	Dimethylether	7.417	2.033	4.69	2.37	126.8	0.1882	35.47
R1234yf	R161	7.954	1.755	4.596	2.009	130.8	0.1641	42.9
R1234yf	R152A	7.812	1.755	4.654	2.013	132.4	0.1657	42.85

R1234yf	R1243zf	7.826	1.755	4.564	2.007	129.8	0.1638	42.93
R1234yf	R290	8.003	1.755	4.47	2.001	127.2	0.1613	43.02
R1234yf	R600	7.638	1.755	4.708	2.016	133.9	0.1673	42.8
R1234yf	R600a	7.659	1.755	4.642	2.012	132.1	0.1659	42.86
R1234yf	R1233zd(E)	7.603	1.755	4.752	2.019	135.2	0.1684	42.76
R1234yf	HFO1336mzz(Z)	7.473	1.755	4.7	2.015	133.7	0.1676	42.81
R1234yf	IsoPentane	7.541	1.755	4.734	2.018	134.7	0.1682	42.78
R1234yf	N-PENTANE	7.494	1.755	4.721	2.017	134.3	0.168	42.79
R1234yf	Cyclohexane	7.642	1.755	4.857	2.026	138.2	0.1705	42.67
R1234yf	Toluene	7.719	1.755	4.913	2.029	139.8	0.1714	42.62
R1234yf	Isohexane	7.496	1.755	4.748	2.019	135.1	0.1686	42.76
R1234yf	Isopropanol	7.717	1.755	4.91	2.029	139.7	0.1714	42.62
R1234yf	n-Hexane	7.42	1.755	4.707	2.016	133.9	0.1679	42.8
R1234yf	n-Heptane	7.506	1.755	4.773	2.02	135.8	0.1691	42.74
R1234yf	Dimethylether	7.804	1.755	4.69	2.015	133.4	0.1665	42.82
R1243zf	R161	7.559	2.033	4.596	2.362	124.3	0.1855	35.55
R1243zf	R152A	7.424	2.033	4.654	2.366	125.8	0.1873	35.5
R1243zf	R1234yf	7.407	2.033	4.428	2.348	119.7	0.1821	35.7
R1243zf	R290	7.606	2.033	4.47	2.351	120.8	0.1823	35.66
R1243zf	R600	7.258	2.033	4.708	2.371	127.3	0.1893	35.46
R1243zf	R600a	7.279	2.033	4.642	2.366	125.5	0.1876	35.51
R1243zf	R1233zd(E)	7.225	2.033	4.752	2.375	128.5	0.1904	35.42
R1243zf	HFO1336mzz(Z)	7.101	2.033	4.7	2.37	127.1	0.1897	35.46
R1243zf	IsoPentane	7.167	2.033	4.734	2.373	128	0.1902	35.43
R1243zf	N-PENTANE	7.122	2.033	4.721	2.372	127.6	0.1901	35.45
R1243zf	Cyclohexane	7.263	2.033	4.857	2.384	131.3	0.1928	35.33
R1243zf	Toluene	7.336	2.033	4.913	2.388	132.8	0.1939	35.28
R1243zf	Isohexane	7.124	2.033	4.748	2.374	128.4	0.1908	35.42
R1243zf	Isopropanol	7.334	2.033	4.91	2.388	132.7	0.1938	35.28
R1243zf	n-Hexane	7.052	2.033	4.707	2.371	127.3	0.19	35.46
R1243zf	n-Heptane	7.133	2.033	4.773	2.377	129.1	0.1913	35.4
R1243zf	Dimethylether	7.417	2.033	4.69	2.37	126.8	0.1882	35.47
R290	R161	7.581	2.015	4.596	2.34	124.6	0.1842	35.95
R290	R152A	7.445	2.015	4.654	2.344	126.2	0.186	35.9
R290	R1234yf	7.428	2.015	4.428	2.326	120.1	0.1808	36.09
R290	R1243zf	7.459	2.015	4.564	2.337	123.7	0.1838	35.97
R290	R600	7.279	2.015	4.708	2.349	127.6	0.1879	35.85
R290	R600a	7.299	2.015	4.642	2.343	125.9	0.1863	35.91
R290	R1233zd(E)	7.246	2.015	4.752	2.352	128.8	0.1891	35.81
R290	HFO1336mzz(Z)	7.121	2.015	4.7	2.348	127.4	0.1883	35.86
R290	IsoPentane	7.187	2.015	4.734	2.351	128.3	0.1889	35.83
R290	N-PENTANE	7.142	2.015	4.721	2.35	128	0.1887	35.84
R290	Cyclohexane	7.283	2.015	4.857	2.361	131.7	0.1914	35.72
R290	Toluene	7.356	2.015	4.913	2.366	133.2	0.1925	35.68
R290	Isohexane	7.144	2.015	4.748	2.352	128.7	0.1894	35.82
R290	Isopropanol	7.354	2.015	4.91	2.366	133.1	0.1924	35.68

R290	n-Hexane	7.072	2.015	4.707	2.349	127.6	0.1887	35.85
R290	n-Heptane	7.153	2.015	4.773	2.354	129.4	0.19	35.79
R290	Dimethylether	7.438	2.015	4.69	2.347	127.1	0.1869	35.87
R600	R161	7.242	2.329	4.596	2.75	119	0.2083	29.65
R600	R152A	7.112	2.329	4.654	2.756	120.5	0.2104	29.6
R600	R1234yf	7.096	2.329	4.428	2.732	114.7	0.2045	29.78
R600	R1243zf	7.126	2.329	4.564	2.746	118.2	0.208	29.67
R600	R290	7.286	2.329	4.47	2.736	115.8	0.2047	29.75
R600	R600a	6.973	2.329	4.642	2.755	120.2	0.2108	29.61
R600	R1233zd(E)	6.922	2.329	4.752	2.767	123.1	0.214	29.52
R600	HFO1336mzz(Z)	6.803	2.329	4.7	2.761	121.7	0.2132	29.56
R600	IsoPentane	6.866	2.329	4.734	2.765	122.6	0.2138	29.53
R600	N-PENTANE	6.823	2.329	4.721	2.763	122.3	0.2136	29.54
R600	Cyclohexane	6.958	2.329	4.857	2.778	125.8	0.2167	29.43
R600	Toluene	7.028	2.329	4.913	2.784	127.2	0.2179	29.39
R600	Isohexane	6.825	2.329	4.748	2.766	123	0.2144	29.52
R600	Isopropanol	7.026	2.329	4.91	2.784	127.2	0.2178	29.39
R600	n-Hexane	6.756	2.329	4.707	2.762	121.9	0.2136	29.56
R600	n-Heptane	6.834	2.329	4.773	2.769	123.6	0.215	29.5
R600	Dimethylether	7.105	2.329	4.69	2.76	121.5	0.2114	29.57
R600a	R161	7.355	2.215	4.596	2.599	120.9	0.1995	31.74
R600a	R152A	7.223	2.215	4.654	2.604	122.4	0.2015	31.69
R600a	R1234yf	7.206	2.215	4.428	2.582	116.5	0.1958	31.88
R600a	R1243zf	7.236	2.215	4.564	2.595	120	0.1992	31.77
R600a	R290	7.4	2.215	4.47	2.586	117.6	0.1961	31.84
R600a	R600	7.062	2.215	4.708	2.609	123.8	0.2036	31.65
R600a	R1233zd(E)	7.029	2.215	4.752	2.614	125	0.2049	31.61
R600a	HFO1336mzz(Z)	6.909	2.215	4.7	2.609	123.6	0.2041	31.65
R600a	IsoPentane	6.973	2.215	4.734	2.612	124.5	0.2047	31.62
R600a	N-PENTANE	6.929	2.215	4.721	2.611	124.2	0.2046	31.64
R600a	Cyclohexane	7.066	2.215	4.857	2.624	127.7	0.2075	31.52
R600a	Toluene	7.137	2.215	4.913	2.63	129.2	0.2086	31.48
R600a	Isohexane	6.931	2.215	4.748	2.613	124.9	0.2053	31.61
R600a	Isopropanol	7.135	2.215	4.91	2.63	129.1	0.2085	31.48
R600a	n-Hexane	6.861	2.215	4.707	2.609	123.8	0.2045	31.65
R600a	n-Heptane	6.94	2.215	4.773	2.616	125.6	0.2059	31.59
R600a	Dimethylether	7.216	2.215	4.69	2.608	123.4	0.2025	31.66
Propylene	R161	7.58	2.016	4.596	2.341	124.6	0.1842	35.93
Propylene	R152A	7.444	2.016	4.654	2.345	126.2	0.1861	35.88
Propylene	R1234yf	7.427	2.016	4.428	2.327	120	0.1808	36.07
Propylene	R1243zf	7.458	2.016	4.564	2.338	123.7	0.1839	35.96
Propylene	R290	7.626	2.016	4.47	2.33	121.2	0.1811	36.04
Propylene	R600	7.278	2.016	4.708	2.35	127.6	0.188	35.84
Propylene	R600a	7.299	2.016	4.642	2.344	125.8	0.1863	35.89
Propylene	R1233zd(E)	7.245	2.016	4.752	2.353	128.8	0.1891	35.8
Propylene	HFO1336mzz(Z)	7.121	2.016	4.7	2.349	127.4	0.1884	35.84

Propylene	IsoPentane	7.186	2.016	4.734	2.352	128.3	0.1889	35.81
Propylene	N-PENTANE	7.141	2.016	4.721	2.351	128	0.1888	35.82
Propylene	Cyclohexane	7.282	2.016	4.857	2.362	131.7	0.1915	35.71
Propylene	Toluene	7.355	2.016	4.913	2.367	133.2	0.1926	35.66
Propylene	Isohexane	7.143	2.016	4.748	2.353	128.7	0.1894	35.8
Propylene	Isopropanol	7.353	2.016	4.91	2.367	133.1	0.1925	35.66
Propylene	n-Hexane	7.071	2.016	4.707	2.35	127.6	0.1887	35.84
Propylene	n-Heptane	7.152	2.016	4.773	2.355	129.4	0.19	35.78
Propylene	Dimethylether	7.437	2.016	4.69	2.348	127.1	0.1869	35.85
R1233zd(E)	R161	7.228	2.344	4.596	2.77	118.8	0.2094	29.39
R1233zd(E)	R152A	7.099	2.344	4.654	2.776	120.3	0.2116	29.34
R1233zd(E)	R1234yf	7.082	2.344	4.428	2.752	114.5	0.2056	29.52
R1233zd(E)	R1243zf	7.112	2.344	4.564	2.766	118	0.2091	29.41
R1233zd(E)	R290	7.272	2.344	4.47	2.756	115.5	0.2058	29.49
R1233zd(E)	R600	6.94	2.344	4.708	2.782	121.7	0.2138	29.3
R1233zd(E)	R600a	6.96	2.344	4.642	2.775	120	0.212	29.35
R1233zd(E)	HFO1336mzz(Z)	6.79	2.344	4.7	2.781	121.5	0.2144	29.3
R1233zd(E)	IsoPentane	6.853	2.344	4.734	2.785	122.4	0.215	29.27
R1233zd(E)	N-PENTANE	6.81	2.344	4.721	2.784	122	0.2148	29.28
R1233zd(E)	Cyclohexane	6.944	2.344	4.857	2.799	125.5	0.2179	29.17
R1233zd(E)	Toluene	7.014	2.344	4.913	2.805	127	0.2191	29.13
R1233zd(E)	Isohexane	6.812	2.344	4.748	2.787	122.7	0.2156	29.26
R1233zd(E)	Isopropanol	7.012	2.344	4.91	2.805	126.9	0.219	29.13
R1233zd(E)	n-Hexane	6.743	2.344	4.707	2.782	121.7	0.2148	29.3
R1233zd(E)	n-Heptane	6.821	2.344	4.773	2.789	123.4	0.2162	29.24
R1233zd(E)	Dimethylether	7.092	2.344	4.69	2.78	121.2	0.2126	29.31
Dimethylether	R161	7.135	2.45	4.596	2.911	117.3	0.2175	27.65
Dimethylether	R152A	7.007	2.45	4.654	2.918	118.7	0.2198	27.61
Dimethylether	R1234yf	6.991	2.45	4.428	2.891	113	0.2136	27.79
Dimethylether	R1243zf	7.02	2.45	4.564	2.907	116.5	0.2172	27.68
Dimethylether	R290	7.179	2.45	4.47	2.896	114.1	0.2138	27.76
Dimethylether	R600	6.851	2.45	4.708	2.925	120.1	0.2221	27.56
Dimethylether	R600a	6.87	2.45	4.642	2.917	118.5	0.2202	27.62
Dimethylether	R1233zd(E)	6.82	2.45	4.752	2.93	121.3	0.2236	27.53
Dimethylether	HFO1336mzz(Z)	6.703	2.45	4.7	2.924	119.9	0.2227	27.57
Dimethylether	IsoPentane	6.764	2.45	4.734	2.928	120.8	0.2234	27.54
Dimethylether	N-PENTANE	6.722	2.45	4.721	2.926	120.5	0.2232	27.55
Dimethylether	Cyclohexane	6.855	2.45	4.857	2.943	123.9	0.2264	27.44
Dimethylether	Toluene	6.924	2.45	4.913	2.949	125.4	0.2276	27.4
Dimethylether	Isohexane	6.724	2.45	4.748	2.929	121.2	0.224	27.53
Dimethylether	Isopropanol	6.922	2.45	4.91	2.949	125.3	0.2275	27.4
Dimethylether	n-Hexane	6.656	2.45	4.707	2.925	120.1	0.2232	27.56
Dimethylether	n-Heptane	6.733	2.45	4.773	2.932	121.8	0.2247	27.51

3.2. Energy and exergy analysis results

Figure 2 shows a representation of the change in turbine power output and ORC thermal efficiency as a function of condenser temperature. Increasing the condenser temperature from 30 °C to 40 °C causes a decrease in turbine power output as well as thermal efficiency. The turbine power output decreases from 10.21 kW to 6.92 kW, while the thermal efficiency decreases from 7.24% to 4.91%. This decrease is caused by an increase in condensation pressure as a result of an increase in temperature. When the temperature of the condenser increases, the pressure of the system at the condenser also increases, thus raising the saturation pressure at the turbine outlet. The increased saturation pressure at the turbine outlet causes a decrease in the pressure ratio between the turbine inlet and outlet, thus reducing the expansion work of the turbine during expansion. This causes a decrease in turbine power output. On the other hand, an increase in condenser temperature causes an increase in the average heat rejection temperature of the ORC, which is known to decrease the thermodynamic efficiency of the cycle. The increased condensation pressure at the turbine outlet causes an increase in the turbine outlet state, thus increasing the specific enthalpy value. This increase causes a decrease in the available enthalpy difference during expansion, thus decreasing turbine power output as well as thermal efficiency.

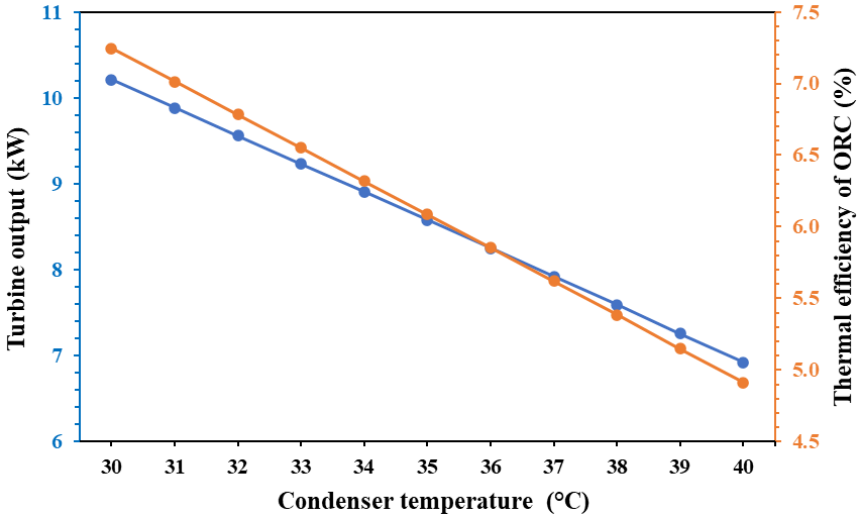

Figure 2. The variation of turbine output and thermal efficiency of ORC with condenser temperature

Figure 3 presents a graph showing the variation of the net COP of the combined ORC and VCC and hydrogen production rate as a function of condenser temperature. As the condenser temperature is increased from 30 °C to 40 °C, there is a gradual reduction in both the hydrogen production rate and the net COP of the ORC and VCC. For instance, the net COP of the combined ORC and VCC reduces from 3.266 to 2.949, whereas the hydrogen production rate reduces from 184.8 g/h to 125.4 g/h. The reduction in COP with increasing condenser temperatures is mainly due to a corresponding increase in condensation pressure of the VCC. When the condenser temperature is increased, it causes a corresponding increase in compressor pressure, leading to an increase in compressor work input. As a result of this increase in compressor work input, there is a reduction in COP of the combined ORC and VCC since the refrigeration capacity is relatively constant while compressor work input is increased. In addition to this, increasing the condenser temperature also adversely affects the ORC since it

causes a reduction in turbine power output, as previously discussed. As a result of this reduction in turbine power output, there is a reduction in electricity generated in the ORC, which is then utilized to drive the hydrogen production reaction in the PEM electrolyzer. As a result of this reduction in electricity generated in the ORC, there is a significant reduction in hydrogen production rate as a function of condenser temperature. From this discussion, it is established that condenser temperature is a significant parameter in ORC, VCC, and PEM systems. Lower condensation temperatures are beneficial to the thermodynamic performance of ORC and VCC since it causes a significant increase in electricity generated in the ORC.

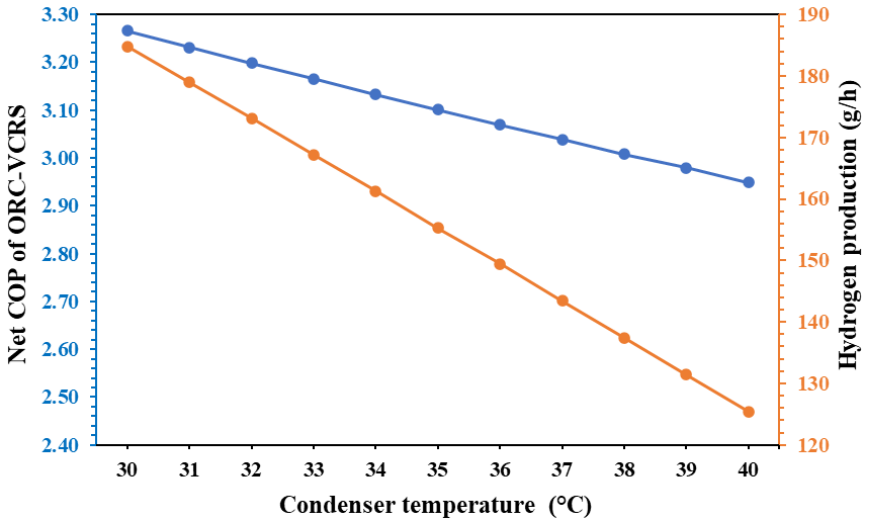

Figure 3. The variation of net COP of ORC-VCC and hydrogen production with condenser temperature

Figure 4 presents the exergy efficiency and total exergy destruction rate of the ORC-VCC-PEM with respect to the condenser temperature. It is evident that when the condenser temperature ranges from 30°C to 40°C, the exergy efficiency of the ORC-VCC-PEM decreases monotonically. At the same time, the total exergy destruction rate increases progressively. More specifically, the exergy efficiency reduces from 27.61% to 22.76%, whereas the total exergy destruction rate increases from 29.77 kW to 27.40 kW. This is mainly caused by the increase in condensation pressure when the temperature in the condenser increases. The high condensation pressure significantly reduces the pressure ratio in the turbine. This reduction causes a significant reduction in the useful output of the ORC. This leads to a reduction in the exergy efficiency of the ORC-VCC-PEM. At the same time, when the condenser temperature increases, the thermodynamic irreversibility in the components of the ORC-VCC-PEM also increases. More specifically, the thermodynamic irreversibility in the compressor of the VCC increases because of the high compressor pressure. Additionally, the thermodynamic irreversibility in the condenser of the ORC increases because of the heat transfer process. This causes the total exergy destruction rate to increase when the temperature in the condenser increases.

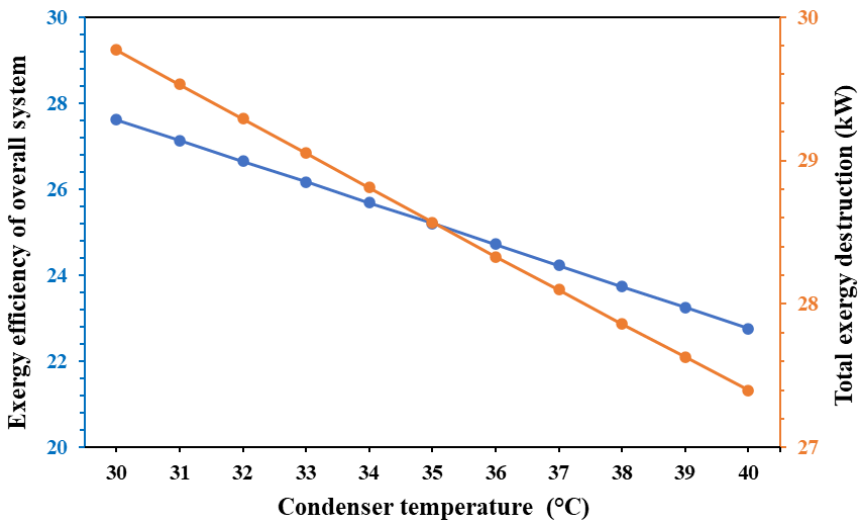

Figure 4. The variation of exergy efficiency of overall system and total exergy destruction rate of ORC with condenser temperature

The change in component-wise exergy destruction rates versus condenser temperature for the integrated ORC-VRC-PEM system is presented in Figure 5. The exergy destruction in the throttling valve is found to be the highest, with a nearly constant exergy destruction rate of 7.754 kW. This is due to the isenthalpic nature of the throttling process, in which there is a pressure drop without any work recovery, leading to exergy destruction. The compressor is found to be the second of exergy destruction, with a nearly constant exergy destruction rate of 6.817 kW over the entire range of temperature. This rate of exergy destruction is mainly due to the irreversible nature of the compression process and high pressure ratios employed in the VCC. The IHE also decreases in exergy destruction from 5.008 kW to 4.621 kW due to a decrease in heat transfer rates with increasing system performance degradation. The exergy destruction in the turbine also decreases from 1.767 kW to 1.159 kW with increasing condenser temperature. This is due to a decrease in turbine pressure ratio with increasing condenser temperature. The exergy destruction in the condenser decreases slightly from 2.38 kW to 2.30 kW with increasing condenser temperature, whereas the exergy destruction in the evaporator is nearly constant at 2.004 kW over all cases, indicating that the refrigeration load is constant. The exergy destruction in the pump is found to be very low, with a value less than 0.01 kW for all cases.

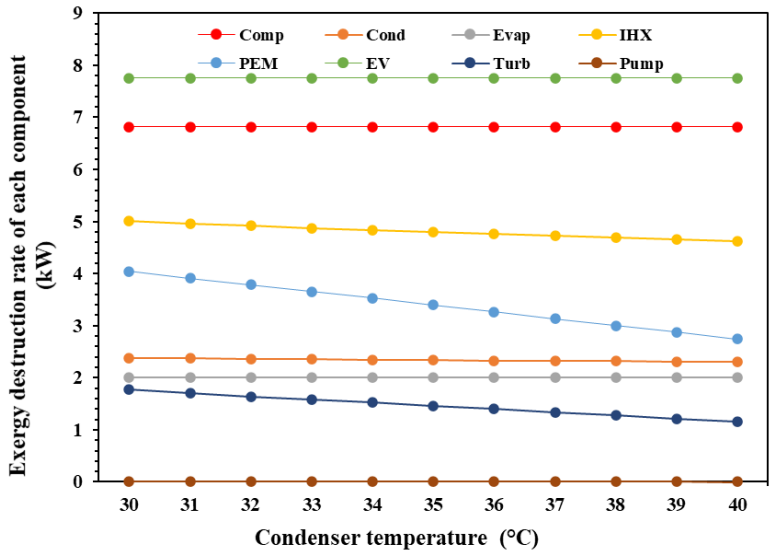

Figure 5. The variation of exergy destruction rate of each component with condenser temperature

Figure 6 presents a graphical presentation of the changes in the power output of the turbine and ORC thermal efficiencies as functions of evaporator temperature. The results show that the evaporator temperature has a minor impact on the ORC. In this regard, increasing the evaporator temperature from 5 to 10°C results in a minor reduction in turbine power output from 6.924 to 6.669 kW, which corresponds to a reduction of 3.82%. This minor reduction in turbine power output is due to an increase in evaporation pressure. As a result, the pressure ratio decreases. Consequently, the enthalpy drop in the turbine decreases. Therefore, the expansion work in the turbine decreases, causing a minor reduction in turbine power output. At the same time, the ORC thermal efficiencies remain invariant at 4.913% throughout the range of evaporator temperatures. This invariance occurs because an increase in evaporator temperature enhances the quality of heat addition in the ORC. However, this enhancement in quality is due to a minor reduction in expansion work in the turbine.

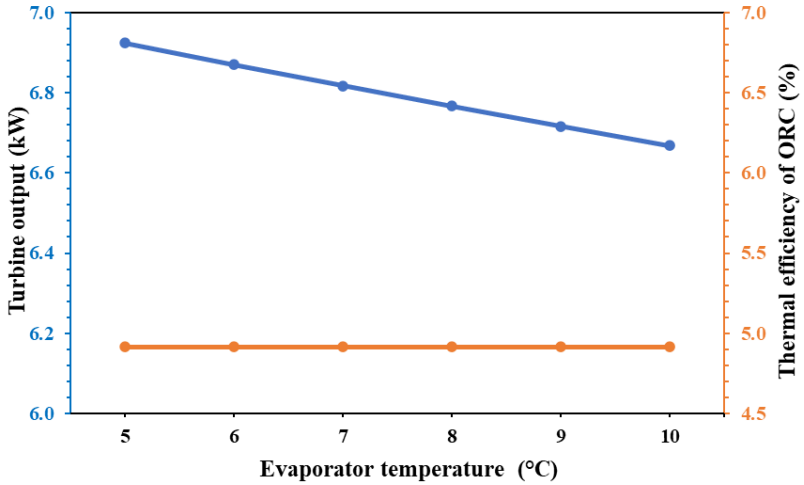

Figure 6. The variation of turbine output and thermal efficiency of ORC with evaporator temperature

Figure 7 illustrates the impact of changes in evaporator temperature on the net COP of the proposed system and hydrogen production rate. From the results presented in Figure 7, it can be seen that an increase in evaporator temperature from 5 to 10 °C results in an enhancement in the net COP of the proposed system from 2.949 to 3.452, reflecting an increase of 17.05%. This enhancement in net COP is mainly due to an increase in evaporator pressure with respect to compressor suction pressure. This causes a reduction in compression ratios. As a result, compressor power is reduced, thus improving the net COP of the proposed system. However, an enhancement in evaporator temperature causes a reduction in hydrogen production rate by 3.89%, from 125.4 g/h to 120.7 g/h. This reduction in hydrogen production rate is mainly due to a reduction in turbine power output caused by a reduction in pressure ratios due to an enhancement in evaporator pressure.

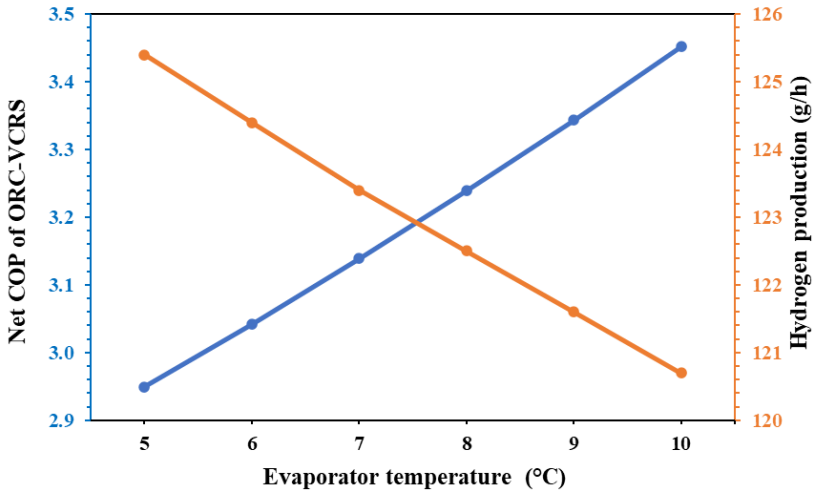

Figure 7. The variation of net COP of ORC-VCC and hydrogen production with evaporator temperature

Figure 8 illustrates the variation of the overall system exergy efficiency and the total exergy destruction rate as functions of the evaporator temperature. As the evaporator temperature increases from 5 °C to 10 °C, the overall exergy efficiency decreases from 22.76% to 20.53%. This is an equivalent reduction of about 10.86%. This reduction is mainly due to a reduction in useful work potential of the cycle, resulting from a reduced differential in temperature between the heat source and the working fluid in the evaporator of the cycle. A reduced differential in temperature reduces the thermodynamic work potential of the cycle, leading to a reduced exergy efficiency of the cycle. On the other hand, there is a reduction in the total exergy destruction rate from 27.40 kW to 24.34 kW, indicating an increase of about 12.57%. This is mainly due to a reduction in pressure ratios of various components of the cycle, especially the compressor and turbine, as the evaporator temperature is increased.

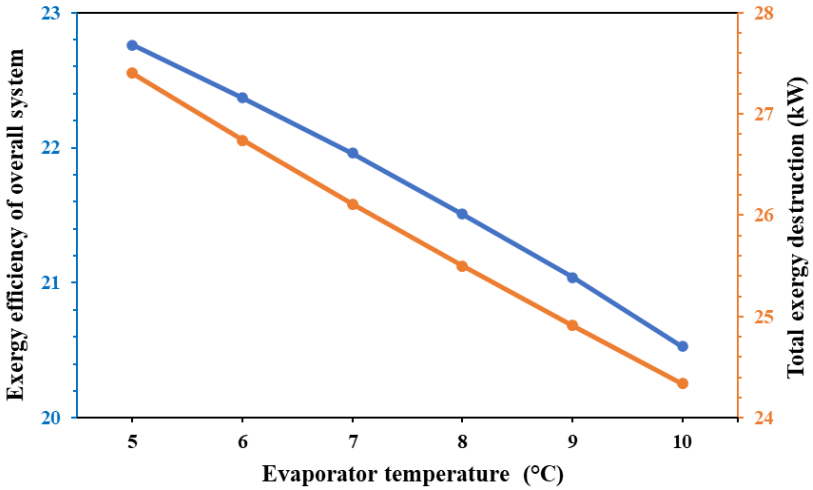

Figure 8. The variation of exergy efficiency of overall system and total exergy destruction rate of ORC with evaporator temperature

Variation of component-wise exergy destruction rates with evaporator temperatures is shown in Figure 9. It is observed that as the evaporator temperature is increased from 5 °C to 10 °C, the exergy destruction of all components decreases progressively, indicating an improvement in the internal thermodynamic efficiency of the system. Although the expansion valve is still the major contributor to irreversibility in the system, there is a decrease in exergy destruction from 7.754 kW to 6.461 kW. This is only an improvement of about 20%. The expansion valve exhibits the highest exergy destruction due to irreversible throttling without work recovery, and its exergy destruction decreases with increasing evaporator temperature because the reduced pressure ratio across the valve lowers entropy generation. The compressor is the second major contributor to irreversibility in the system. The exergy destruction of this component decreases significantly as the evaporator temperatures are increased. The exergy destruction of this component decreases significantly from 6.817 kW to 5.645 kW as the evaporator temperatures are increased. This is mainly due to an increase in evaporating pressure, which decreases the compression ratio and hence reduces the entropy generation during compression. All other components, including the PEM, condenser, evaporator, IHE, and turbine, also show moderate decreases in exergy destruction due to decreases in pressure ratio and hence lower entropy generation during heat transfer and expansion processes. The pump is still contributing negligibly to irreversibility.

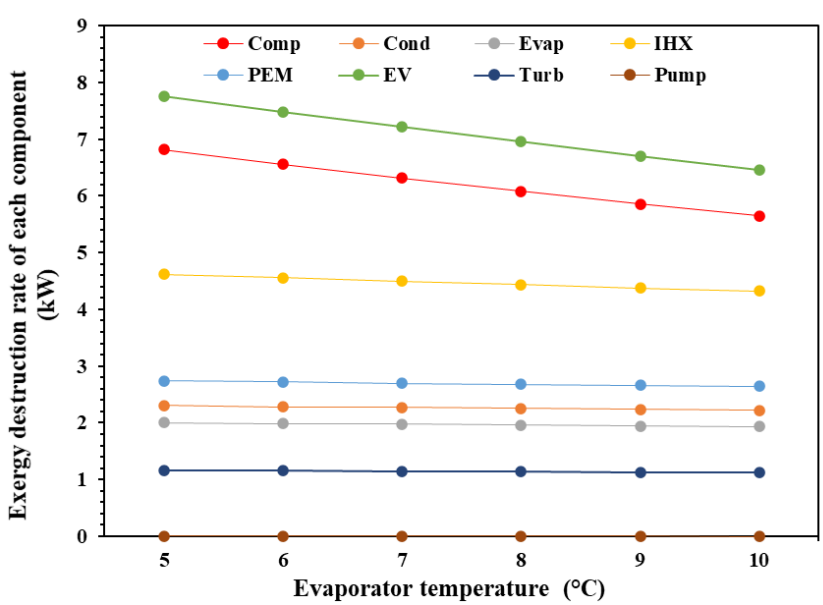

Figure 9. The variation of exergy destruction rate of each component with evaporator temperature

Figure 10 shows the influence of the temperature differential within the IHE on turbine power output and ORC efficiency. As the temperature differential within the IHE increases from 5 to 15 °C, turbine power output as well as ORC efficiency decreases. From 8.443 kW to 5.325 kW, turbine power output decreases as the temperature difference increases within the IHE. Moreover, ORC efficiency decreases from 5.99% to 3.779% as the temperature difference ranges from 5 to 15 °C. This indicates that turbine power output decreases by 58.51%, while ORC efficiency decreases by 58.55%. This could be attributed to the reduction in heat transfer efficiency within the IHE as the temperature difference increases. A higher temperature difference between hot and cold streams within the IHE results in a reduction in heat transfer efficiency. This results in a reduction in the degree of superheating of the working fluid entering the turbine. As a result, there is a reduction in the degree of enthalpy drop.

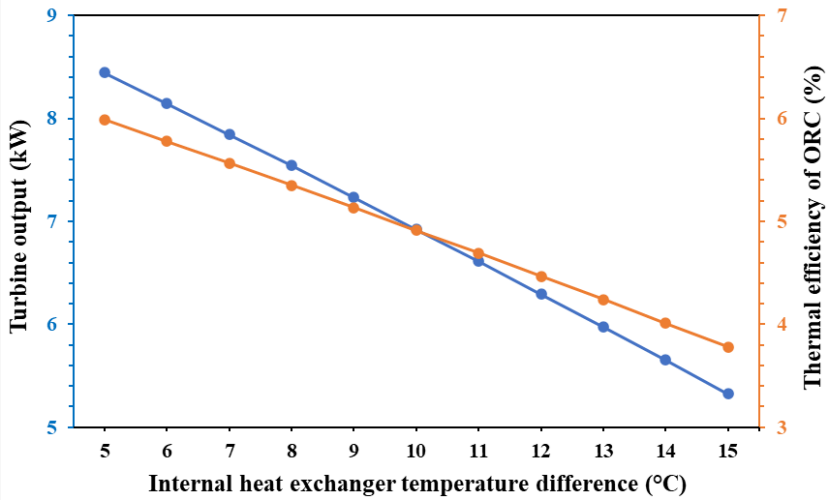

Figure 10. The variation of turbine output and thermal efficiency of ORC with internal heat exchanger temperature difference

Figure 11 demonstrates the effect of the IHE temperature difference on the performance of the refrigeration and hydrogen production in the integrated ORC-VCC-PEM system. As shown in Figure 11, with an increase in the IHE temperature difference from 5 °C to 15 °C, the net COP of the ORC-VCC is reduced from 3.088 to 2.817, indicating a reduction of around 9.62%. This reduction is mainly caused by the deterioration in performance of the IHE in terms of internal heat recovery, which in turn leads to degradation in the thermodynamic quality of the working fluid supplied to the turbine. This degradation in turbine power causes an increase in compressor work in the refrigeration cycle, resulting in reduced performance in terms of COP. Similar behavior is observed in hydrogen production rate, where it is significantly reduced with an increase in IHE temperature difference. From 152.9 g/h to 96.43 g/h, hydrogen production is reduced by around 58.56%. This is due to the reduction in turbine power output with an increase in IHE temperature difference. As mentioned in the above paragraph, since the PEM is driven by electricity generated in the turbine, any reduction in turbine power output would reduce the hydrogen production rate. Therefore, it is concluded that with an increase in IHE temperature difference, hydrogen production rate is reduced.

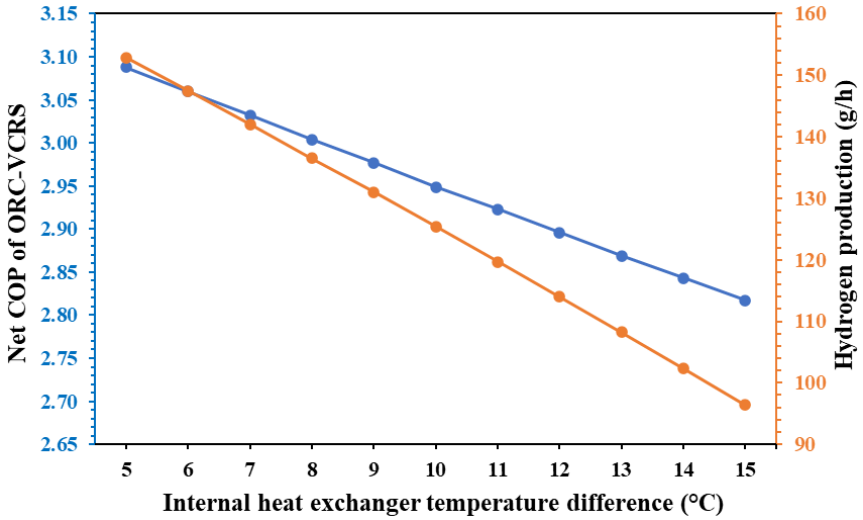

Figure 11. The variation of net COP of ORC-VCR and hydrogen production with internal heat exchanger temperature difference

Figure 12 shows the impact of the IHE temperature difference on the total exergy efficiency and total exergy destruction of the integrated ORC-VCC-PEM system. As the IHE temperature difference increases from 5 °C to 15 °C, the total exergy efficiency decreases from 19.68% to 17.84%. The efficiency drops by around 9.4%. This is mainly due to the decrease in heat transfer efficiency within the IHE. The larger temperature difference reduces the efficiency of heat transfer within the IHE, hence reducing the quality of the working fluid entering the turbine and hence decreasing the amount of work available. At the same time, the total exergy destruction increases slightly from 37.11 kW to 37.95 kW as the temperature difference increases from 5 °C to 15 °C. The exergy destruction increases by around 2.3%. This is mainly due to increased entropy generation within the system as the heat transfer efficiency within the IHE decreases. The decrease in efficiency within the internal heat exchanger increases irreversibility within various components of the system, hence increasing the total exergy destruction of the integrated system.

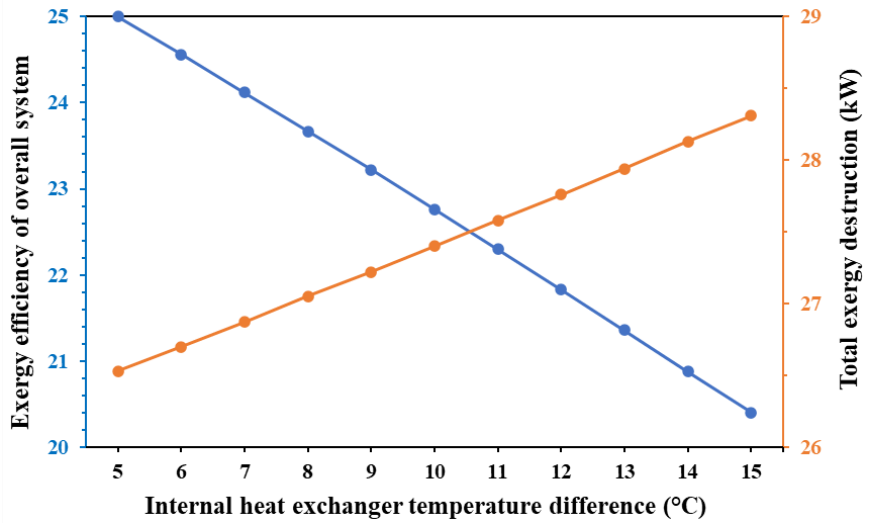

Figure 12. The variation of exergy efficiency of overall system and total exergy destruction rate of ORC with internal heat exchanger temperature difference

Variations in component-wise exergy destruction rates as a function of IHE temperature difference are presented in Figure 13. As the IHE temperature difference is increased from 5 °C to 15 °C, there is a significant change in the distribution of exergy destruction rates among system components. The expansion valve is again identified as the major contributor to irreversibility in the system, with constant exergy destruction rates of 7.754 kW over the entire range of operation. There is a significant increase in exergy destruction rates within the IHE, which increases sharply from 2.921 kW to 6.41 kW, i.e., an increase of 120%. This is related to the worsening of internal heat transfer, which increases with increases in temperature difference. There are significant decreases in exergy destruction rates within the PEM electrolyzer and turbine. The exergy destruction rate within the PEM decreases from 3.342 kW to 2.109 kW, and the exergy destruction rate within the turbine decreases from 1.411 kW to 0.893 kW. The decreases can be attributed to the decrease in turbine power output as the IHE temperature difference is increased. The remaining components, i.e., the condenser, evaporator, and pump, show varying changes in exergy destruction rates, with the pump showing negligible contributions to irreversibility. The results show that there is significant amplification of irreversibility within the IHE and decreases in irreversibility within the turbine and PEM electrolyzer as the IHE temperature difference is increased.

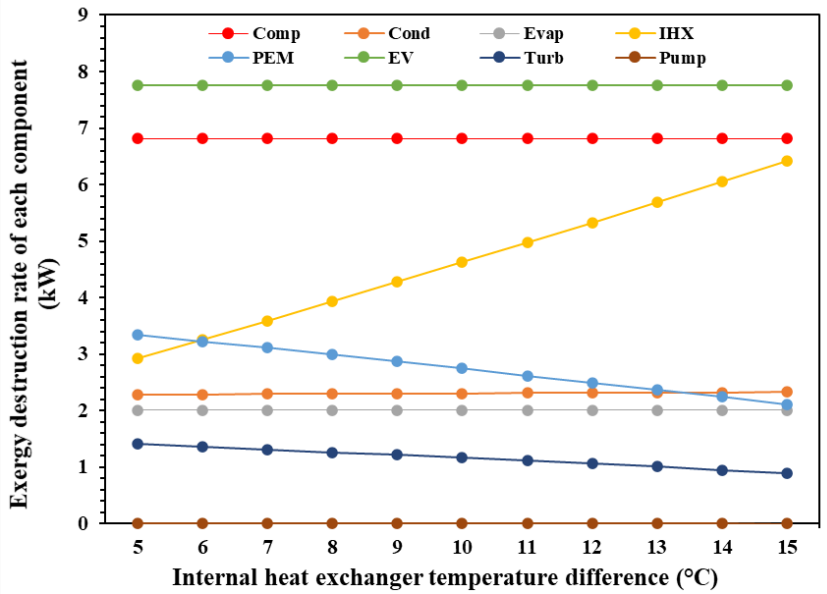

Figure 13. The variation of exergy destruction rate of each component with internal heat exchanger temperature difference

3.3. Strategies for reducing exergy destruction

The results obtained from the analysis indicate that the overall exergy performance of the ORC-VCC-PEM system is largely influenced by the expansion valve, compressor, and IHE, as these are the primary sources of exergy destruction. The expansion valve was seen to have the highest exergy destruction among all the components of the system, mainly due to the presence of irreversible processes in the throttling device without any provision of work recovery. Thus, replacing the throttling device by using an expander or ejector configuration is seen as a viable option for enhancing the overall performance of the ORC-VCC-PEM. Besides, enhancing the compressor isentropic efficiency as well as reducing the compressor pressure ratio significantly reduces the compressor-related exergy destruction. It was also seen that the IHE was functioning as a cascade heat exchanger between the ORC-VCC, thus playing a critical role in the overall exergy performance of the ORC-VCC-PEM. Further analysis of the results obtained from the analysis shows that excessive temperature differences in the IHE component result in higher entropy generation, thus indicating the importance of designing the IHE component of the system in an optimum manner. Besides, it was seen that higher evaporator temperatures result in reduced exergy destruction in the expansion device as well as the overall system, while higher condenser temperatures tend to increase compressor-related exergy destruction as well as marginally reducing exergy destruction in the thermal components of the system, including the turbine, PEM, and IHE component of the system.

4.Conclusion

The present study offers a thorough thermodynamic assessment of the proposed tri-generation system, consisting of an ORC, a VCC, and a PEM-based electrolyzer. Out of 188 combinations of working fluids, the combination of Dimethylether (VCC) and Toluene (ORC) has been found to be the optimal combination. Therefore, this combination of working fluids has been employed for all the parametric investigations carried out in this study.

- The performance of the ORC–VCC–PEM system is strongly governed by evaporator temperature, condenser temperature, and IHE temperature difference, with clear impacts on both system efficiency and component-wise irreversibilities.
- Increasing evaporator temperature from 5 °C to 10 °C improves system performance, yielding a ~17.1% increase in COP_{net} and a ~11.2% reduction in total exergy destruction, while simultaneously reducing exergy destruction in all major components, particularly the compressor (~17.2%), expansion valve (~16.7%), and IHE (~6.4%).
- Increasing condenser temperature from 30 °C to 40 °C causes a ~9.7% decrease in COP_{net}, a ~32.1% decrease in hydrogen production rate, and a ~7.9% decrease in exergy efficiency, while slightly reducing exergy destruction in thermal components (IHE ↓~7.7%, PEM ↓~32.2%, turbine ↓~34.4%) but maintaining high irreversibility in the expansion valve and compressor.
- Increasing IHE temperature difference from 5 °C to 15 °C leads to a ~8.8% decrease in COP_{net} and a ~6.7% increase in total exergy destruction, mainly due to a ~119% increase in IHE-related irreversibility (2.921 → 6.41 kW), despite reductions in PEM (~36.9%) and turbine (~36.7%) exergy destruction.
- Component-wise analysis confirms that the expansion valve is the dominant source of exergy destruction (~7.75 kW, nearly constant), followed by the compressor (~6.82 kW) and IHE, while the pump contribution remains negligible.
- The IHE functions as a cascade heat exchanger coupling the ORC and VCC subsystems, and excessive temperature differences significantly intensify entropy generation, making its optimization critical.
- The hydrogen production rate is the most sensitive output parameter, particularly to condenser temperature, indicating strong thermo-electrochemical coupling within the system.
- Overall, optimal system performance is achieved by operating at higher evaporator temperatures, lower condenser temperatures, and moderate IHE temperature differences, together with advanced strategies such as throttling loss recovery, compressor efficiency enhancement, and optimized cascade heat exchange.

Ethics in Publishing

There are no ethical issues regarding the publication of this study.

Author Contributions

The author solely conducted the investigation, conceptualization, system design, data collection, analysis, and interpretation, and was fully responsible for writing and revising the manuscript.

References

[1] Drescher, U., & Brüggemann, D. (2007). Fluid selection for the Organic Rankine Cycle (ORC) in biomass power and heat plants. Applied Thermal Engineering, 27(1), 223–228.

[2] Pili, R., Martínez, L., Wieland, C., et al. (2020). Techno-economic potential of waste heat recovery from German energy-intensive industry with Organic Rankine Cycle technology. Renewable and Sustainable Energy Reviews, 134, 110324.

[3] Roumpedakis, C., Loumpardis, G., Monokrousou, E., et al. (2020). Exergetic and economic analysis of a solar driven small scale ORC. Renewable Energy, 157, 1008–1024.

[4] Eyerer, S., Dawo, F., Wieland, C., et al. (2020). Advanced ORC architecture for geothermal combined heat and power generation. Energy, 205, 117967.

[5] Xu, W. C., Deng, S., Zhao, L., et al. (2018). How to quantitatively describe the role of the pure working fluids in subcritical organic Rankine cycle: A limitation on efficiency. Energy Conversion and Management, 172, 316–327.

[6] Sang-Chan, P., Chang-Hyo, S., Ho-Saeng, L., et al. (2023). Performance analysis of an organic Rankine cycle with an internal heat exchanger considering turbine pressure ratio and efficiency. Energy, 285, 129507.

[7] Jiang, S. J., & Wei, Z. W. (2024). Urbanization exacerbated the rapid growth of summer cooling demands in China from 1980 to 2023. Sustainable Cities and Society, 106, 105382.

[8] Coulomb, D. (2008). Refrigeration and cold chain serving the global food industry and creating a better future: Two key IIR challenges for improved health and environment. Trends in Food Science & Technology, 19(8), 413–417.

[9] Zhar, R., Allouhi, A., Ghodbane, M., et al. (2021). Parametric analysis and multi-objective optimization of a combined Organic Rankine Cycle and Vapor Compression Cycle. Sustainable Energy Technologies and Assessments, 47, 101401.

[10] Javanshir, N., Mahmoudi, S., & Rosen, M. (2019). Thermodynamic and exergoeconomic analyses of a novel combined cycle comprised of vapor-compression refrigeration and organic rankine cycles. Sustainability, 11(12), 3374.

[11] Nasir, M., & Kim, K. (2016). Working fluids selection and parametric optimization of an Organic Rankine Cycle coupled Vapor Compression Cycle (ORC-VCC) for air conditioning using low grade heat. Energy and Buildings, 129, 378–395.

[12] Li, H. S., Bu, X. X., Wang, L. B., et al. (2013). Hydrocarbon working fluids for a Rankine cycle powered vapor compression refrigeration system using low-grade thermal energy. Energy and Buildings, 65, 167–172.

[13] Rami, Y., & Allouhi, A. (2024). 3E (Energy, Exergy and Economic) multi-objective optimization of a novel solar-assisted ocean thermal energy conversion system for integrated electricity and cooling production. Energy Conversion and Management, 321, 119006.

[14] Xia, X. X., Liu, Z. P., Wang, Z. Q., et al. (2023). Multi-layer performance optimization based on operation parameter–working fluid–heat source for the ORC-VCR system. Energy, 272, 127103.

[15] Wang, Z. K., Li, Y. M., Qiu, Z. J., et al. (2025). Thermodynamic and economic analysis of a novel dual-pressure organic Rankine cycle coupled two-stage vapor compression heat pump system. International Journal of Refrigeration, 172, 240–255.

[16] Karellas, S., & Braimakis, K. (2016). Energy–exergy analysis and economic investigation of a cogeneration and trigeneration ORC–VCC hybrid system utilizing biomass fuel and solar power. Energy Conversion and Management, 107, 103–113.

[17] Qureshi, M., Chandio, M., Memon, A., et al. (2024). Thermal analysis of solar energy based organic Rankine cycle cascaded with vapor compression refrigeration cycle. Energy Nexus, 14, 100291.

[18] Xia, X. X., Liu, Z. P., Wang, Z. Q., et al. (2023). Energy, conventional and advanced exergy analysis for the organic Rankine cycle–vapor compression refrigeration combined system driven by low-grade waste heat. Applied Thermal Engineering, 220, 119650.

[19] Asim, M., Khan, S., Khan, S. A., et al. (2025). Thermal analysis and optimal fluid selection for the novel integrated vapor compression cycle and ORC system for ultra-low grade waste heat recovery using the desuperheating method. Energy Nexus, 17, 100357.

[20] Nasir, M. T., Ali, M. A., Khanc, T. S., et al. (2019). Performance assessment and multi-objective optimization of an Organic Rankine Cycle driven cooling air conditioning system. Energy and Buildings, 191, 13–30.

[21] Saleh, B. (2018). Energy and exergy analysis of an integrated organic Rankine cycle–vapor compression refrigeration system. Applied Thermal Engineering, 141, 697–710.

[22] Wang, Z. Q., Yi, Q. H., Zhao, Y. B., et al. (2025). Parameter analysis and multi-objective optimization of organic Rankine cycle coupled vapor compression cycle using PSO-BPNN model. Applied Thermal Engineering, 273, 126583.

[23] Sun, J., Liu, L. L., Zhang, T., et al. (2025). Optimization and comparative analysis of various organic Rankine cycle-based integrated systems for cooling and power cogeneration utilizing waste heat. Energy Conversion and Management, 325, 119328.

[24] Barac, A., Živić, M., Virag, Z., et al. (2024). Thermo-economic multi-objective optimisation of a solar cooling system. Renewable and Sustainable Energy Reviews, 202, 114656.

[25] Malwe, P. D., Shaikh, J., Gawali, B. S., Panchal, H., Dalkilic, A. S., Rahman, S., & Alrubaie, A. J. (2022). Dynamic simulation and exergy analysis of an Organic Rankine Cycle integrated with vapor compression refrigeration system. Sustainable Energy Technologies and Assessments, 53, 102684.

[26] Gholamian, E., Habibollahzade, A., Zare, V. (2018). Development and multi-objective optimization of geothermal-based organic Rankine cycle integrated with thermoelectric generator and proton exchange membrane electrolyzer for power and hydrogen production. Energy Conversion and Management, 174, 112-125.

[27] Soyturk, G., Kizilkan, O., Ezan, M. A., Colpan, C. O. (2023). PVT integrated hydrogen production with small-scale transcritical power cycle. Process Safety and Environmental Protection, 180, 351-360.